REVISTA MEXICANA DE FÍSICA **46 SUPLEMENTO 2**, 79–83 NOVIEMBRE 2000

Preparation and characterizacion of functional and non-functional nanocomposites

U. Pal, J. García Serrano, A. Bautista Hernández, O. Vázquez Cuchillo, and E. Aguila Almanza
Instituto de Física, Universidad Autónoma de Puebla
Apartado postal J-48, 72570 Puebla, Pue., Mexico

N. Koshizaki and T. Sasaki
National Institute of Materials and Chemical Research (NIMC) AIST, MITI,
1-1 Higashi, Tsukuba, Ibaraki 305, Japan.

Recibido el 27 de abril de 2000; aceptado el 15 de junio de 2000

Functional nanocomposites like Si/ZnO, Au/ZnO and non-functional nanocomposites like Cu/SiO_2 were prepared either by r.f. co-sputtering or by ion-implantation technique. The composite films were prepared with different compositions and thermally treated at different temperatures to study the variation of their optical properties with composition and annealing temperature. X-ray diffraction (XRD), transmission electron microscopy (TEM), and transmission electron diffraction (TED) techniques were used for their structural characterization. Formation of colloidal metal particles and the semiconductor clusters in the matrix have been confirmed by TEM, TED and spectrophotometric measurements.

Keywords: Nanoparticles; metal and semiconductors; optical properties

Nanocompósitos funcionales tales como Si/ZnO, Au/ZnO y no-funcionales como Cu/SiO_2 fueron preparados por las técnicas de co-*sputering* r.f. o por implantación iónica. Las películas compósitas fueron preparadas con diferentes composiciones y tratadas a diferentes temperaturas para estudiar la variación de sus propiedades ópticas con su composición y temperatura del tratamiento. Se han usado las técnicas tales como difracción de rayos X (XRD), microscopía electrónica de transmisión (TEM) y difracción de electrones por transmisión (TED) para su caracterización estructural. Se han confirmado la formación de partículas coloidales metálicas y cúmulos semiconductores en la matriz por mediciones de TEM, TED y espectrofotométricas.

Descriptores: Nanopartículas; metales y semiconductores; propiedades ópticas

PACS: 61.46.+w; 61.82.Rx; 78.66.Vs

1. Introduction

In recent years, the preparation and characterization of low dimensional semiconductor and metal composites have attracted much interest due to their strong photoluminescence (PL) in the visible and near infrared (IR) regions [1–5], and non-linear optical properties [6] respectively. The semiconductor dispersed nanocomposites have modofied optical properites and are highly prosperous materials for the fabrication of optoelectronic devices and chemical sensors [7]. By incorporating semiconductors in glass matrix in different ways, several optical functional composites have been prepared and the mechanism of the origin of optical functionalities in them are being studied extensively at present. However, the use of functional matrix materials like ZnO, MgO for the preparation of nanocomposites is very recent [8–10]. On the other hand, incorporation of low dimensional metal particles in glass matrix using several techniques is being studied to investigate the mechanism of their formation and effect of post growth treatments on them.

In the present project, we took the assignment to prepare several functional and non-functional nanocomposites like Si/ZnO, Au/ZnO, Cu/SiO_2 etc. and to study their structural and optical properties to investigate their applicability in optoelectronic devices and chemical sensors. Though, apart from the above mentioned three materials we are preparing other materials like Cu/ZnO, GaAs/SiO_2 etc. we will restrict ourselves on the discussion of only the previously mentioned three materials.

2. Experimental

Si/ZnO and Au/ZnO composite films were prepared on quartz glass substrates by co-sputtering of Si ($5 \times 5 \times 0.3$ mm^3) wafers or 3 pieces of Au (of different lengths like 1 mm, 3 mm and 7 mm) wires and ZnO (100 mm diameter) targets with 100 W r.f. power. For Si/ZnO composites, the films were prepared at 10 mTorr Ar pressure. Whereas, the Au/ZnO composites were prepared at 4 mTorr Ar pressure. The content of Si and Au in the films were varied by changing the number of Si co-targets or by changing the length of Au wires on the ZnO target, keeping the time of sputtering fixed (60 minutes). The as-deposited Si/ZnO composite films were annealed at different temperatures (400–800°C) for 5 hours in vacuum (2×10^{-6} Torr) and the Au/ZnO composite films were annealed at different temperatures (320–700°C) in argon atmosphere. The content of Si and Au in the composite films were determined by a Perkin-Elmer (PHI 5600ci) XPS

system. X-ray diffraction, TEM and TED techniques were used for the structural characterization of the films. For TEM and TED observations, the composite films of about 25 nm thickness with different Si/Au contents were deposited on carbon-coated NaCl substrates. The films after transferring to the copper grids were annealed at different temperatures and inspected by a JEOL JEM2000-FXII electron microscope. A SHIMADZU (UV3101PC) double beam spectrophotometer was used for the measurement of optical absorption in the films. A Nicolet Magna 750 FTIR spectrometer was used to record the IR absorption spectra of Si/ZnO composites in diffuse mode.

The Cu/SiO_2 composites were prepared by implanting 2.0 MeV Cu^+ ions in fused quartz glass substrates using a 3 MeV Tandem accelerator. Keeping the ion current fixed to 1.5 μA, the samples were prepared with different nominal doses like 5×10^{15} (sample a), 9×10^{15} (sample b), and 1×10^{16} (sample c) ions/cm^2. Rutherford backscattering spectrometry (RBS), using 4.0 MeV He^+ ions has been employed to study the depth profiles of Cu in the substrates after implantation. For the analysis of depth profiles, the program RUMP (Rutherford universal maipulation program) [11], in combination with the results of RBS measurements have been used. Optical absorption measurements were dome at room temperature in the interval of 190 to 700 nm using an un-implanted substrate as reference.

3. Results and discussion

Si/ZnO

The Si/Zn atomic ratio was calculated from the $Si2_{P3/2}$ and $Zn2_{P3/2}$ peak areas in XPS spectra of the films. Content of Si in the films increased with the increase of Si pieces and could easily be controlled by changing the number of Si pieces on the ZnO target.

Figure 1 shows the typical micrographs of as-deposited and 800°C annealed Si/ZnO films. For the as-deposited films we can observe the nanoparticles of size ranging from 2 to 4 nm dispersed in the matrix. On annealing at 700°C or higher temperatures, the nanoparticles aggregated to form bigger clusters (micro-clusters there after). In Fig. 1b we can see the micro-clusters of 10 to 60 nm size (average size 34 nm) formed after annealing the film at 800°C. The average size of the clusters did not depend much on the Si content in the films. However, their number density increased with the increase of Si content in the films.

The position of the $Si2_p$ emission in the XPS spectra varied from 101.6 to 102.8 eV which is in between the peak positions of elemental Si (99.2 eV) and SiO_2 (103.9 eV). So, in the clusters, Si remained apparently in the SiO_X ($0 < X < 2$) chemical state.

IR absorption spectra of the films revealed several peaks in the 400–700 cm^{-1} spectral range. There appeared a broad non-symmetric peak for all the samples, the position of which varied systematically with the variation of Si content and the

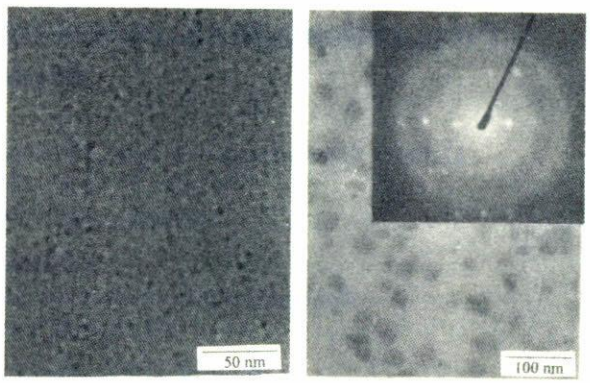

FIGURE 1. Typical TEM micrographs of (a) as-grown and (b) 800°C annealed Si/ZnO films prepared with same Si content. Insert of (b) shows the TED pattern taken on a micro-cluster.

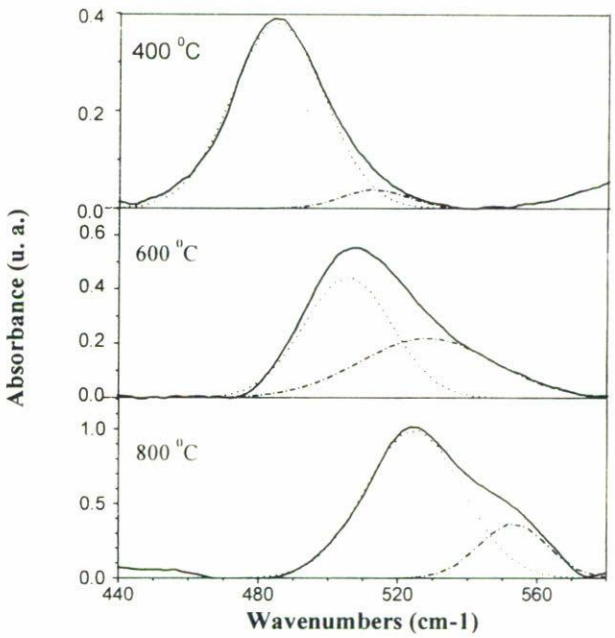

FIGURE 2. Evolution of IR absorption peak with annealing temperature ans its computer-simulated decompositions, for a Si/ZnO film prepared with 16 Si co-targets.

temperature of annealing of the films. A computer-simulated decomposition of these complex peaks showed two adjacent bands in them, the position of which vary with the content of Si in the films and also with the temperature of annealing. In Fig. 2, the evolution of the peak with the variation of annealing temperature, and their computer-simulated decomposition are presented. Both the component bands moved towards shorter wavelength with the increase of annealing temperature. The longer wavelength side band moved from 485 to 525 cm^{-1}, whereas the shorter wavelength band moved from 512 to 550 cm^{-1}. We assign these two sets of bands to the Si-Si stretching asymmetric (SA) and stretching symmet-

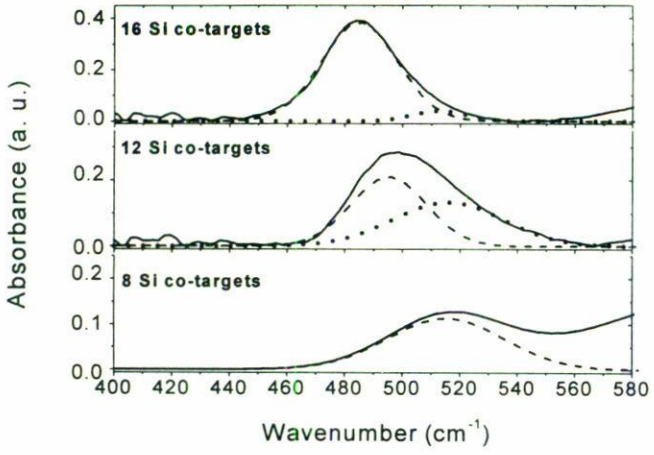

FIGURE 3. IR absorption spectra for Si/ZnO composite films with different Si contents, annealed at 400°C.

ric (SS) vibrations [11] in Si_3 clusters, respectively. A reverse effect is observed on increasing the Si content in the films. With the increase of Si content, the absorption peak shifted towards longer wavelength. With the increase of Si content, the intensity of the peak increased sharply and its position shifted from 517 to 480 cm^{-1}. The absorption at about 485 and 508 cm^{-1} correspond to the triplet excited states $^3B_1$ (C_{2v}) and $^3A_2$ (D_{3h}) of Si_3, respectively [12]. The peaks appeared at about 525 and 550 cm^{-1} correspond to the absorption of singlet ground state $^1A_1$(C_{2v}) of Si_3. So, as the temperature of annealing increased, the configuartion of the Si atoms in Si_3 clusters changed from the triplet to the singlet ground state. The 507 and 532 cm^{-1} absorptions (Fig. 3) correspond to the most stable triplet $^3A_1$(C_{2v}) state of isosceles structure and the second most stable triplet state of linear chain structure of Si_3, respectively [13]. So, as the Si content in the films increased, the Si_3 cluster in the films acquired the lesser stable geometrical structure.

Au/ZnO

In Fig. 4, XRD spectra of the as-deposited films with different Au contents are shown. With the increase of Au content, the intensity of the (220), (331) and (422) peaks of Au increased. There appeared a peak corresponding to the formation of AuO, intensity of which also increased with the increase of Au content in the films.

In Fig. 5, the TEM micrographs of the composite films with same Au content but annealed at different temperatures are shown. Formation of Au nanoparticles in the films is clear. With the increase of annealing temperature, the average size of the Au particles increased.

Formation of nanometric Au particles in the films is also evident from their optical absorption spectra. In Fig. 6, optical absorption spectra of a film prepared with 3 pieces of 7 mm length Au wires and annealed at different temperatures are shown. The appearance of a hump near about 2.3 eV in the spectra corresponds to plasmon absorption in the small

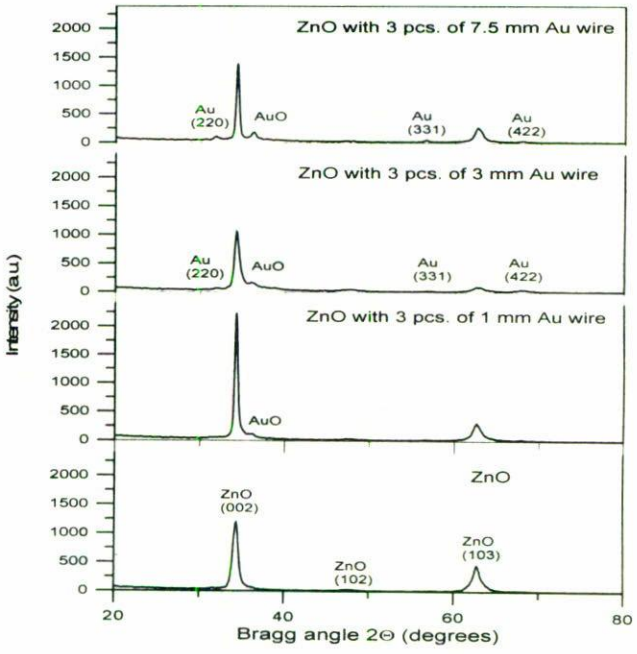

FIGURE 4. X-ray diffraction spectra for Au/ZnO composites prepared with different Au contents.

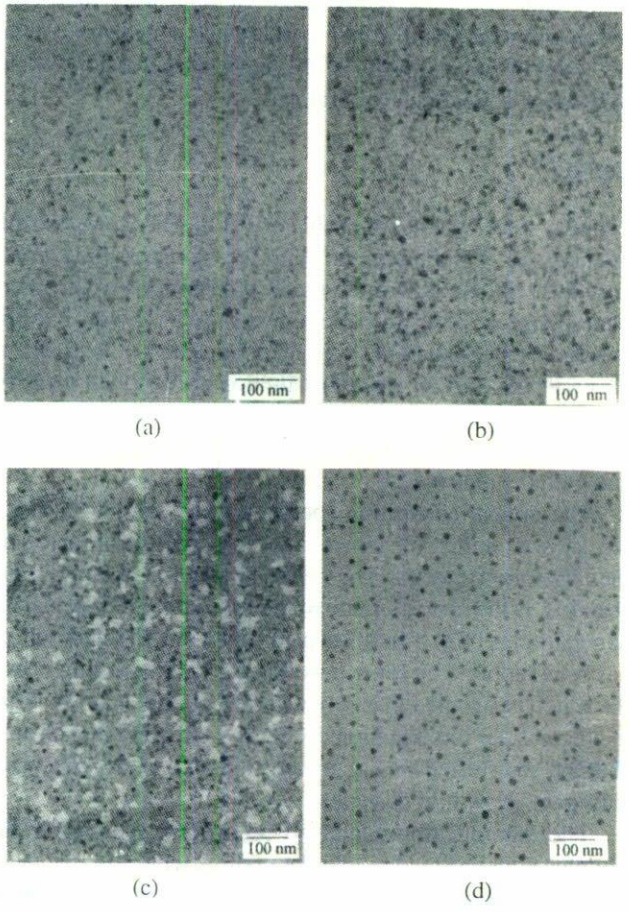

FIGURE 5. TEM micrographs of (a) as-grown, (b) 320°C, (c) 500°C and (d) 700°C annealed Au/ZnO films prepared with 3 pieces of 7 mm Au co-targets.

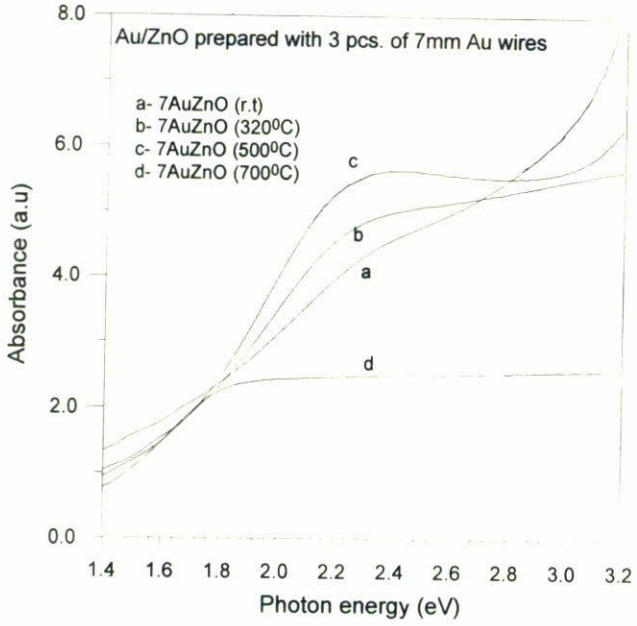

FIGURE 6. Optical absorption spectra of a Au/ZnO composite film annealed at different temperatures.

Au particles. The plasmon absorption peak shifted towards lower energy as the temperature of annealing increased; which is in agreement with the observations made from TEM study that the average size of Au particles increases with the increase of annealing temperature.

Cu/SiO_2

Figure 7 shows the depth profile of Cu in silica glass for different doses of implantation. With the increase implantation dose the principal distribution of Cu becomes sharper, more intense and its position shifts towards lower depths. On the increase of implantation dose, there appeared other peaks at lower depths, and the main distribution transformed from the bimodal to a Gaussian one. These behaviors can be explain by considering the interaction the Cu ions among themselves and with the matrix [14].

The optical absorption spectra for the samples a and b are shown in Fig. 8. There appeared two clear peaks in the absorption spectra. The peak appeared at about 560 nm (band 1), is the characteristic of the formation of colloidal Cu nanoparticles [15]. The other peak close to 215 nm (band 2), has been reported by several workers [15, 16] and assigned to the E'defect in silica glass created during implantation. With the increase of implantation dose, the band 1 became clearer, sharper, and shifted slowly towards higher wavelengths, indicating the growth of particles.

The theoretically calculated absorption spectra for the samples are presented by the data points with different symbols in the same figure (Fig. 8). For the simulation of optical absorption spectra, we used the Maxwell-Garnett theory with "mean free path" correction for the dielectric function of the nanoparticles. The details of this models can be found in

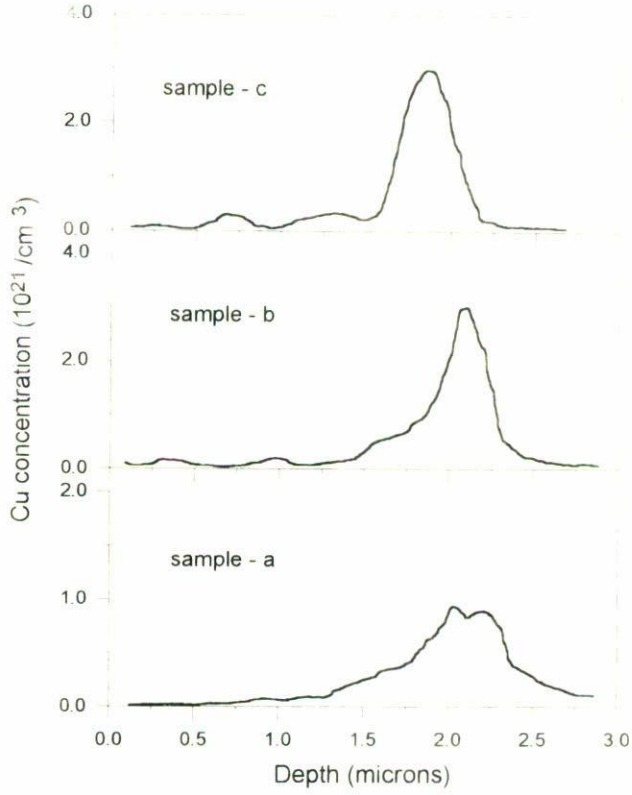

FIGURE 7. Depth profiles of Cu in silica glass for different implantation doses.

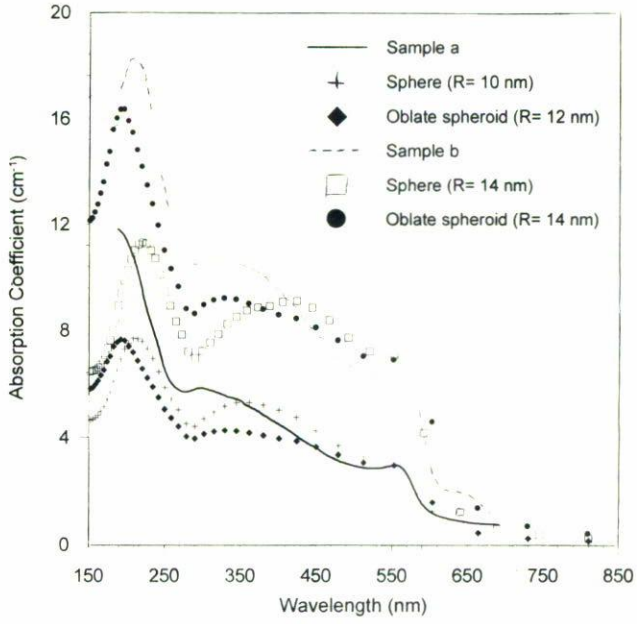

FIGURE 8. Absorption spectra of Cu/SiO_2 samples (a and b) and their theoretical fits.

Ref. 17. The simulations are realized by taking two forms of the particle, spheres and oblate spheroids. For the sample a, prepared with lower implantation dose, the theoretical fitting is better when the spherical shape of the particles

is considered. On the other hand, for the samples prepared with higher implantation dose, the theoretical spectra fitted well with the experimental spectra when an oblate spheroidal shape of the particles is considered. In the samples prepared with lower implantation dose, as the average size of the particles is small, a spherical shape for them is expected. With the increase of implantation dose, the Cu particles grow, and probably take some irregular form deviating from their regular spherical shape.

4. Conclusions

Si and Au clusters can be prepared in ZnO matrix by r.f. co-sputtering technique. The Si clusters, formed in Si/ZnO composites, consist of a core of Si_3 and a SiO_X cap layer around them.

Au nanoparticles formed in ZnO matrix remain mostly in its elemental state with an oxide layer at the particle-matrix interface. The size of the nanoparticles can be controlled by controlling either by the content of Au in the films or by controlling the temperature of annealing.

Distribution of Cu in silica depends on the implantation dose. With the increase of implantation dose, Cu segregate towards substrate surface. For the samples prepared with low implantation dose, the size of the Cu particles is very small and the natural spherical shape retain in them. With the increase of implantation dose, the size of the Cu particle increase and their shape deviate from spherical to oblate spheroidal.

Acknowledgments

We are thankful to Dr. L. Rodriguez-Fernández and Dr. J.C. Chean-Wong for preparing Cu/SiO_2 samples and their RBS analysis. The work is supported by CONACyT (Grant no. 28380-E), Mexico.

1. S. Hayashi, M. Kataoka, and K. Yamamoto, *J. Appl. Phys.* **32** (1993) 274.
2. S. Yoshida, T. Handa, S. Tanabe, and N. Soga, *Jpn. J. Appl. Phys.* **35** (1996) 2694.
3. Y. Maeda *et al.*, *Appl. Phys. Lett.* **59** (1991) 3168.
4. Y. Kanzawa *et al.*, *Solid State Commun.* **102** (1997) 533.
5. S. Hayashi, T. Nagareda, Y. Kanzawa, and K. Yamamoto, *Jpn. J. Appl. Phys.* **32** (1993) 3840.
6. R.H. Haglund *et al.*, *Nucl. Instr. and Meth. Phys. Res. B* **91** (1994) 493.
7. N. Koshizaki, K. Yasumoto, and S. Terauchi, *Jpn. J. Appl. Phys.* **34** (suppl. 34-1) (1994) 119.
8. N. Koshizaki *et al.*, *Nanostruct. Mater.* **8** (1997) 403.
9. U. Pal, N. Koshizaki, S. Terauchi, and T. Sasaki, *Microsc. Microanal. Microstruct.* **8** (1997) 403.
10. G. Zhao, H. Kozuka, and T. Yoko, *Thin Solid Films* **227** (1996) 147.
11. S. Li, R.J. Van Zee, W. Weltner Jr., and K. Raghavachari, *Chem. Phys. Lett.* **243** (1995) 275.
12. C.M. Rohlfing and K. Raghavachari, *J. Chem. Phys.* **96** (1992) 2114.
13. R. Fournier, S.B. Sinnott, and A.E. DePristo, *J. Chem. Phys.* **97** (1992) 4149.
14. A. Bautista-Hernández, U. Pal, L. Rodriguez-Fernández, and J.C. Cheang-Wong, *Superficies y Vacio* **9** (1999) 296.
15. P. Mazzoldi, F. Caccavale, P. Chakraborty, R.A. Zhur, and G. Whichard, *J. Non-Crys. Sol.* **129** (1991) 46.
16. R.H. Magruder III *et al.*, *J. Appl. Phys.* **76** (1994) 708.
17. R. Ruppin, *J. Appl. Phys.*, **59** (1986) 1355.